nature catalysis

Article

https://doi.org/10.1038/s41929-025-01392-9

Electrosynthesis of ethylene glycol from ethylene coupled with CO_2 capture

Received: 22 March 2024

Accepted: 7 July 2025

Published online: 18 August 2025

Check for updates

Rong Xia[1,2,6], Yiqing Chen[1,2,6], Yuxin Chang[3], Heejong Shin[1,2], Huajie Ze[1,2], Hengzhou Liu[1,2], Pengfei Ou[1,2], Roham Dorakhan[3], Sungjin Park[3], Panos Papangelakis[3], Zunmin Guo[3], Eduardo G. Machado[4], Marcio V. Reboucas[4], Mohsen Nikkhoo[5], Ricardo G. A. Duarte[4], Daojin Zhou[1,2], Yuan Liu[2], Weiyan Ni[1,2], Cong Tian[1,2], Yuanjun Chen[1,2], Christine Yu[1], Omar K. Farha[1], Ke Xie[1,2] ✉ & Edward H. Sargent[1,2] ✉

Current ethylene glycol (EG) production generates 46 million metric tons of CO_2 equiv. emission annually. While electrified synthesis could decarbonize this process, existing ethylene oxidation systems suffer from high energy consumption resulting from excessive voltages. Here we identify, with the aid of in situ photoluminescence spectroscopy, an increased pH at the membrane–anode interface within a membrane–electrode assembly electrolyser and find that it arises due to hydroxide counter-migration across the membrane. To address this challenge, we integrate cathodic electrochemical carbon capture to reduce hydroxide flux and develop $RuSnO_x$ catalysts that favour *Cl over *OH adsorption, facilitating chloride-mediated ethylene oxidation. The system achieves 94% Faradaic efficiency for ethylene-to-EG conversion and 91% CO_2 capture efficiency from a 10% CO_2 stream, sequestering 0.60 tonnes CO_2 per tonne of EG produced from ethylene. This approach results in an estimated carbon intensity of 0.133 tonnes CO_2 equiv. per tonne EG, compared with the global average of 1.2 tonnes CO_2 equiv. per tonne EG.

Ethylene glycol (EG), a key component in polyester fibres, plastics and antifreeze, had a market size of 30 million metric tons per year in the year 2022[1,2]. Today, its production relies mainly on the oxidation of ethylene to ethylene oxide, at temperatures of 200–300 °C and pressures of 1.5–2.5 MPa, followed by the hydrolysis of ethylene oxide at 120–250 °C and 1–4 MPa (refs. 3,4). This process generates 46 million metric tons of CO_2 emissions annually[1,5]. Of the average 1.2 tonnes CO_2 per tonne EG, 0.8 tonnes come from ethylene production, and 0.4 tonnes come from the overoxidation of ethylene during ethylene oxide manufacture[6–10].

The electrification of EG production is thus of interest. Recent advancements have achieved a 76% Faradaic efficiency for EG production via formaldehyde electroreduction[5], operating at a full cell voltage of 3.2 V and a current density of 100 mA cm^{-2}. Ethylene, nevertheless, is, for the moment, the dominant feedstock in use, the result of its global availability. Prior studies on direct ethylene electrooxidation have reached an 80% EG Faradaic efficiency but were limited to 10 mA cm^{-2} current densities[5,6,11,12]. Indirect (mediated) ethylene partial oxidation produces ethylene oxide, a precursor to EG, at a higher current density (>100 mA cm^{-2}). This has a full cell voltage that exceeds 4 V, resulting in notable energy consumption of ~15.5 GJ per tonne EG from the electrolysis step alone, still appreciable compared with the total 22.6 GJ per tonne EG in traditional thermocatalytic methods. A key challenge is designing the electrochemical interface to maintain

[1]Department of Chemistry, Northwestern University, Evanston, IL, USA. [2]Department of Electrical and Computer Engineering, Northwestern University, Evanston, IL, USA. [3]Department of Electrical and Computer Engineering, University of Toronto, Toronto, Ontario, Canada. [4]Braskem S.A., Polo II de Alta Tecnologia, Condomínio Globaltech, Campinas, Paulínia, Brasil. [5]Braskem America, Pasadena, TX, USA. [6]These authors contributed equally: Rong Xia, Yiqing Chen. ✉e-mail: ke-xie@northwestern.edu; ted.sargent@northwestern.edu

high selectivity while minimizing the internal resistance within the electrolyser with the goal of lowering overall energy consumption.

In this study, we used in situ photoluminescence spectra to explore the electrochemical interface during chloride-mediated ethylene oxidation in a membrane–electrode assembly (MEA) electrolyser. Despite a strongly acidic bulk pH in the anolyte, we found that the microenvironment at the membrane–anode interface was near neutral, the result of OH^- counter-migration across the membrane. As a result, although the MEA design reduces energy consumption by lowering internal resistance, the near-neutral local environment at the membrane–anode interface decreases ethylene oxidation selectivity by favouring the competing oxygen evolution reaction. This observation highlighted an undesired trade-off between ethylene oxidation Faradaic efficiency and energy consumption.

This led us to explore the use of the process of CO_2 capture on the cathodic side to consume OH^- and offset the effects of the undesired hydroxide counter-migration. Previous studies used pH gradients for electrochemical carbon capture—often relying on organic redox-active mediators or bipolar membranes[13,14]. The former is limited to low current densities (<10 mA cm^{-2}) and sensitivity to oxygen, while the latter relies on bipolar membranes and solid electrolytes, with the best reported full cell voltage of 1.9 V at 100 mA cm^{-2} (refs. 15–18). The present study instead takes advantage of the pH gradient in ethylene oxidation using a cation-exchange membrane-based microfluidic electrolyser for carbon capture and operates at 1.8 V and 100 mA cm^{-2}. We further developed tin-doped RuO_2 that favours *Cl adsorption over *OH, shifting the selectivity towards chloride-mediated ethylene under near-neutral environment in the paired electrolyser and achieve a 94% Faradaic efficiency for chloride-mediated ethylene oxidation. We find that, in cathodic carbon capture, the system achieves a 91% carbon capture efficiency when we employ a 10% CO_2 stream, and this enables it to sequester 0.60 tonnes of CO_2 per tonne of EG produced. This configuration lowers the total energy consumption of the system to 10 GJ per tonne EG (of which 6.6 GJ are due to the electrolysis step), compared with 22.6 GJ per tonne EG for the existing thermocatalytic route. The electrified approach offsets in part the carbon intensity of ethylene from fossil feedstock, leading to an estimated carbon intensity of 0.13 tonnes CO_2 equiv. per tonne EG, compared with the 1.2 tonnes CO_2 equiv. per tonne EG global average for EG today.

Results

Local microenvironment impact on ethylene partial oxidation

In initial studies, we fabricated a zero-gap MEA electrolyser; our purpose was to study and improve the ethylene partial oxidation reaction using a chloride-mediated mechanism (Fig. 1a and Supplementary Fig. 1, schematics of MEA). We provide NaCl electrolyte on each side and use RuO_2 for chloride-mediated ethylene partial oxidation at the anode and obtained an encouraging full cell voltage of 2.7 V at 100 mA cm^{-2}; this compared with the 4.5 V observed in the conventional three-compartment flow cell (Fig. 1b). The cathodic reaction with which we paired the anodic process was the hydrogen evolution reaction (HER), for which we used Pt/C as the catalyst. Unfortunately, the Faradaic efficiency was only 42% towards ethylene chlorohydrin in the MEA configuration.

We noted that the local pH at the anode catalyst is expected to impact the relative rates of the desired chloride oxidation for mediated ethylene oxidation versus the undesired oxygen evolution reaction. In our studies, we used the neutral electrolyte NaCl. During the electrolysis, the catholyte is expected to alkalify and the anolyte to acidify as Na^+ transport across the cation-exchange membrane and the reduction reaction produces OH^-, while chloride oxidation yields hydrochloric acid and hypochlorous acid (Supplementary Note 1).

It would be important to evaluate the actual local pH at the membrane–anode interface under operando conditions. After we operated the device for 30 min continuously, the bulk pH of the anolyte descended to 1.5 (measured using a pH meter). To study the local pH at the membrane–anode interface, we used in situ photoluminescence based on a pH-sensitive dye anchored onto the membrane (see Supplementary Note 2 for pH-sensitive dye method). After subtracting the background from the spectra collected during the in situ photoluminescence experiment, we found that the local pH at the membrane–anode interface is in the range of 5–6 (Fig. 1c and Supplementary Fig. 3).

We noted the large [OH^-] gradient across the membrane: this could potentially lead to OH^- diffusion, from cathode to anode, and could account for the local alkalinity on the anode side of the membrane. Indeed such counter-migration has been observed by others under analogous conditions[19].

This possibility motivated us to study pH effects on the anodic ethylene oxidation. Rotating ring–disc electrode (RRDE) measurements (Fig. 1d and Supplementary Fig. 4) in pH 1 versus pH 6 showed that, in acidic conditions, the desired chloride oxidation reaction in mediated ethylene oxidation is the predominant reaction. By contrast, at pH 6, the oxygen-evolution reaction (OER) overtakes chloride oxidation. We propose that competitive adsorption occurs between hydroxide and chloride ions on the catalyst surface, and that—in the presence of a high local [OH^-] concentration—hydroxide adsorption leads to oxygen evolution.

Coupling CO_2 capture at cathode to suppress OH^- counter-migration

We contemplated whether a cathodic reaction—an alternative to an HER—might suppress OH^- counter-migration, which we posited was leading to the competitive adsorption between hydroxide and chloride ions on the anode catalyst. Better yet, we looked for an application that took advantage of and consumed this local flux of OH^- on the cathodic side of the membrane.

CO_2 capture appeared to be a promising such reaction: it would benefit from OH^- generation, leading to carbonate formation in the catholyte, and would consume OH^- and thus limit the diffusive flux across the membrane.

We implemented the oxygen reduction reaction (ORR) reaction to produce OH^- using iron single-atom catalysts (Fe–N–C) (Supplementary Figs. 5–10) and proceeded to estimate, experimentally, the CO_2 capture efficiency: the ratio of OH^- consumed to convert CO_2 into carbonate to the number of cathodically generated hydroxide ions (Methods). While the anode is in direct contact with membrane, we introduced ~2 mm microfluidic channel between cathode and membrane to prevent salt precipitation.

We achieved a CO_2 capture efficiency of 91% at current density of 100 mA cm^{-2}. This was obtained when we used a gas feed stream composed of 10% CO_2, 20% O_2 and 70% N_2. Gas chromatography and ^{1}H nuclear magnetic resonance (NMR) spectroscopy revealed no detectable hydrogen or CO_2 reduction products—an expected result given that the oxygen reduction reaction is more favourable than CO_2 electroreduction/HER.

When comparing ethylene oxidation paired with carbon capture versus hydrogen evolution in a microfluidic electrolyser, introducing CO_2 into the cathode gas inlet led to a pH (Fig. 1e) of 11.4 instead of 13.7 in the prior case of an HER. Pairing ethylene partial oxidation on the anode with ORR for CO_2 capture on the cathode decreased the full cell voltage by over 1 V (Fig. 1e). When comparing the full cell voltage of ethylene oxidation coupled with ORR, both with and without carbon capture (Supplementary Fig. 11), we observed a decrease in cell voltage when carbon capture was implemented. This decrease can be attributed to a reduction in the pH gradient across the membrane, which in turn reduces the associated Nernst loss. Most strikingly, the Faradaic efficiency for anodic ethylene partial oxidation increased from 40% to 71%, consistent with the hypothesis that using OH^-—with the goal of lowering [OH^-] supply on the cathode side of the membrane and thus lowering the pH gradient at the membrane interface—improved local conditions on the anode towards ethylene partial oxidation (Fig. 1f).

https://doi.org/10.1038/s41929-025-01392-9

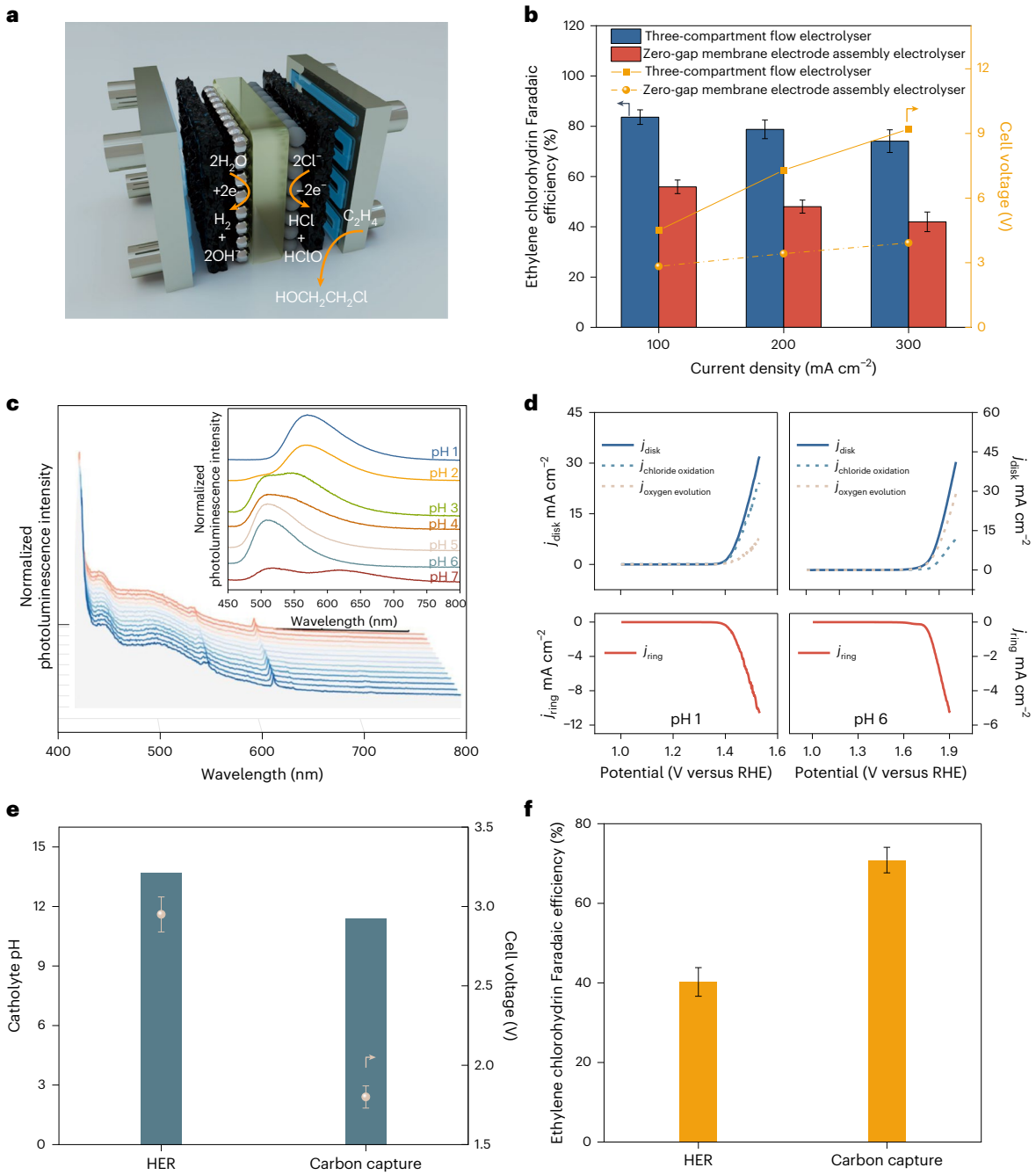

Fig. 1 | Effect of the local microenvironment on electrochemical ethylene partial oxidation. a, Reaction mechanism of chloride-mediated ethylene partial oxidation in a MEA electrolyser. **b**, A comparison of ethylene partial oxidation in a three-compartment flow electrolyser and zero-gap MEA electrolyser. **c**, In situ photoluminescence study of local pH at the membrane–anode interface under reaction conditions. The inset shows the photoluminescence spectra of LSG dye under various pH levels. **d**, RRDE experiment employing RuO_2 under acidic and near-neutral conditions to distinguish the oxygen evolution reaction and the chloride oxidation reaction. **e**, Cathodic pH when conducting an HER and carbon capture in microfluidic electrolyser at 100 mA cm^{-2}. Carbon capture is performed in a gas mixture of 10% CO_2, 20% O_2 and 70% N_2. **f**, Anodic Faradaic efficiency of ethylene partial oxidation when coupled with an HER versus with carbon capture in microfluidic electrolyser at 100 mA cm^{-2}. Data are mean and s.d. from triplicate measurements ($n = 3$).

Anodic catalyst design to maximize chloride-mediated ethylene oxidation

Since even the improved Faradaic efficiency of 71% left considerable room for improvement, we pondered whether the catalyst could be better designed to prefer chloride oxidation over oxygen evolution under near-neutral condition. We used the density functional theory (DFT) to study the chlorine evolution reaction (ClER) versus OER selectivity of RuO_2 (110) and $RuMO_x$ (110) (where M is V, W or Sn) by calculating the Gibbs free energy of chlorine ($\Delta G_{*O\rightarrow *OCl}$) and hydroxyl ($\Delta G_{*O\rightarrow *OOH}$) adsorption at pH 5 (Supplementary Notes 3 and 4, Supplementary Figs. 16–21 and Supplementary Tables 2 and 3). We find a nearly linear scaling relationship between $\Delta G_{*O\rightarrow *OCl}$ and $\Delta G_{*O\rightarrow *OOH}$ (Supplementary Fig. 12) and further find dopants have a more pronounced effect on *OH over *Cl. Specifically, Sn doping slightly increases $\Delta G_{*O\rightarrow *OCl}$ but markedly raises $\Delta G_{*O\rightarrow *OOH}$, shifting selectivity from OER to ClER, making $RuSnO_x$ the most promising candidate for ClER at a near-neutral pH. $RuSnO_x$ is also projected to decrease Pourbaix energy and increase stability during chloride oxidation (Supplementary Figs. 14 and 15).

https://doi.org/10.1038/s41929-025-01392-9

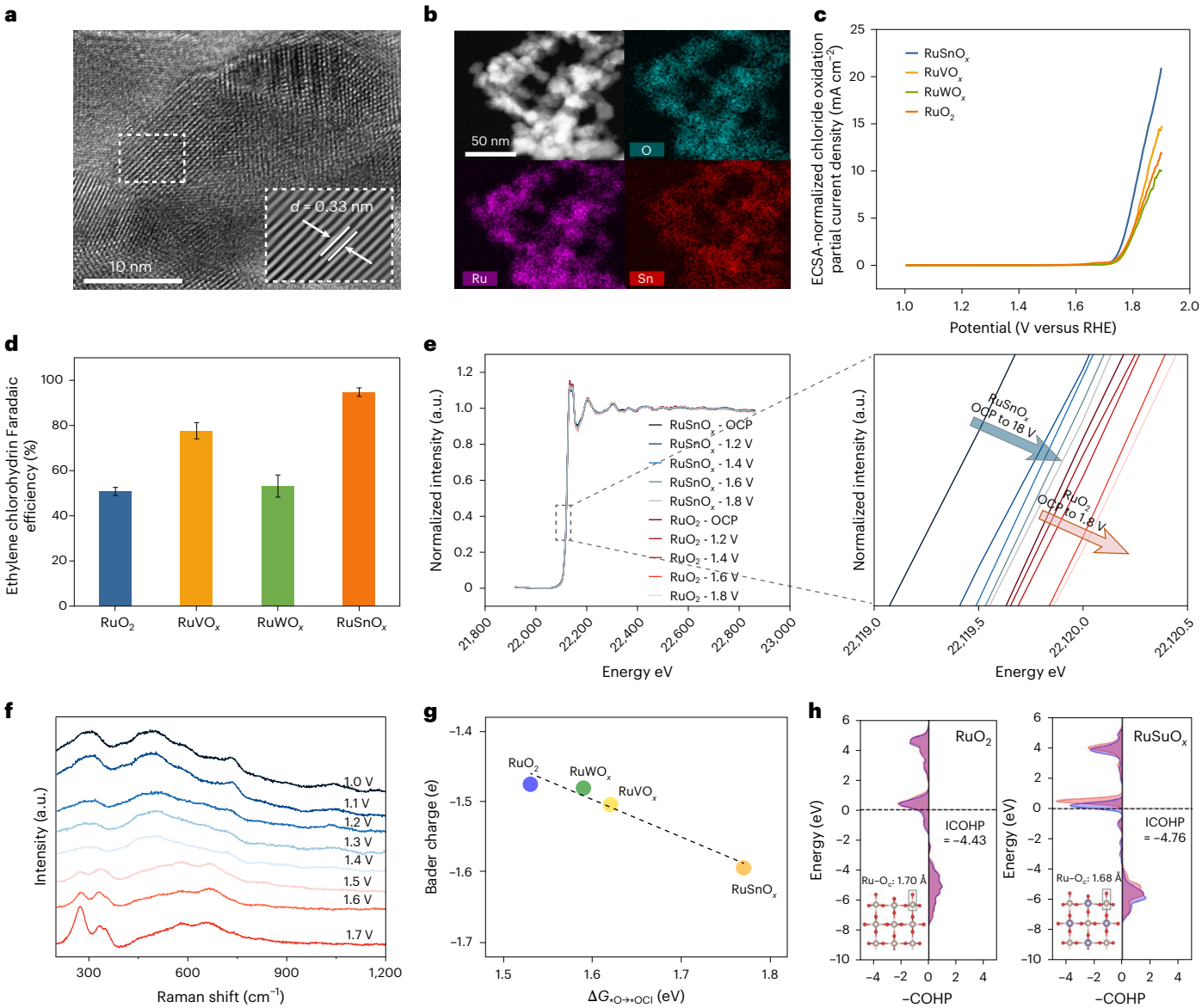

Fig. 2 | RuO_2-based mixed oxide catalysts for ethylene oxidation under near-neutral conditions. a, High-resolution TEM image of $RuSnO_x$. **b**, Energy dispersive spectroscopy mapping of $RuSnO_x$. **c**, ECSA-normalized chloride oxidation partial current density of $RuMO_x$ catalysts identified by an RRDE experiment under neutral conditions. **d**, Ethylene chlorohydrin Faradaic efficiency of $RuMO_x$ catalysts at a constant potential of 1.8 V versus RHE. **e**, In situ Ru K edge XANES spectra of $RuSnO_x$ and RuO_2 under the applied potentials ranging from 1.0 to 1.8 V versus RHE. OCP, open-circuit potential. **f**, In situ surface-enhanced Raman spectra of $RuSnO_x$ at various potential ranging from 1.0 to 1.7 V versus RHE. **g**, Bader charge of preadsorbed O_c and $\Delta G_{*O\rightarrow *OCl}$ of RuO_2 (110) and $RuMO_x$ (110) (where M is V, W or Sn). **h**, COHP analysis of the Ru–O_c bond strength in RuO_2 and $RuSnO_x$. The blue and red lines represent the COHPs for the majority and minority spin, respectively. Data are mean and s.d. from triplicate measurements ($n = 3$).

Experimentally we synthesized candidate catalysts using a hydrothermal method[20] (Fig. 2a,b and Supplementary Fig. 22). Within the family considered in DFT, $RuMO_x$ (where M is Sn, V or W), $RuSnO_x$ exhibited the highest electrochemical active surface area (ECSA)-normalized chloride oxidation partial current density in RRDE screening (Fig. 2c and Supplementary Fig. 23). We further tested the $RuMO_x$ for chloride-mediated ethylene oxidation at a constant potential of 1.8 V versus the reversible hydrogen electrode (RHE). $RuSnO_x$ had a Faradaic efficiency of 94% for ethylene chlorohydrin production (Fig. 2d), the highest among catalysts evaluated. When we analysed the gaseous product using gas chromatography, we observed no measurable CO_2, indicating that overoxidation of ethylene was substantially avoided in chloride-mediated ethylene partial oxidation. We conducted cyclic voltammetry studies in a non-chloride electrolyte (Supplementary Fig. 24). There are no appreciable differences with versus without ethylene, and no ethylene oxidation products were detected in the liquid electrolyte. These findings suggest that ethylene oxidation occurs through a chloride-mediated pathway in the solution rather than directly on the catalyst surface. ^{13}C-labelled ethylene was applied to investigate any 1,2-dichloroethane formation (Supplementary Fig. 25). The ^{13}C-NMR results suggest that 2-chloroethanol is the only product of chloride-mediated ethylene oxidation.

We sought to understand, with the aid of in situ X-ray absorption spectroscopy (XAS), the chemical origins of the increased operating stability of $RuSnO_x$ relative to RuO_2. Across the wide range of applied anodic potentials from 1.0 to 1.8 V, ruthenium in $RuSnO_x$ is in a lower oxidation state than it is in RuO_2 under the same operating conditions (Fig. 2e). The addition of Sn thus appears to militate against overoxidation known to contribute to the degradation of RuO_2.

https://doi.org/10.1038/s41929-025-01392-9

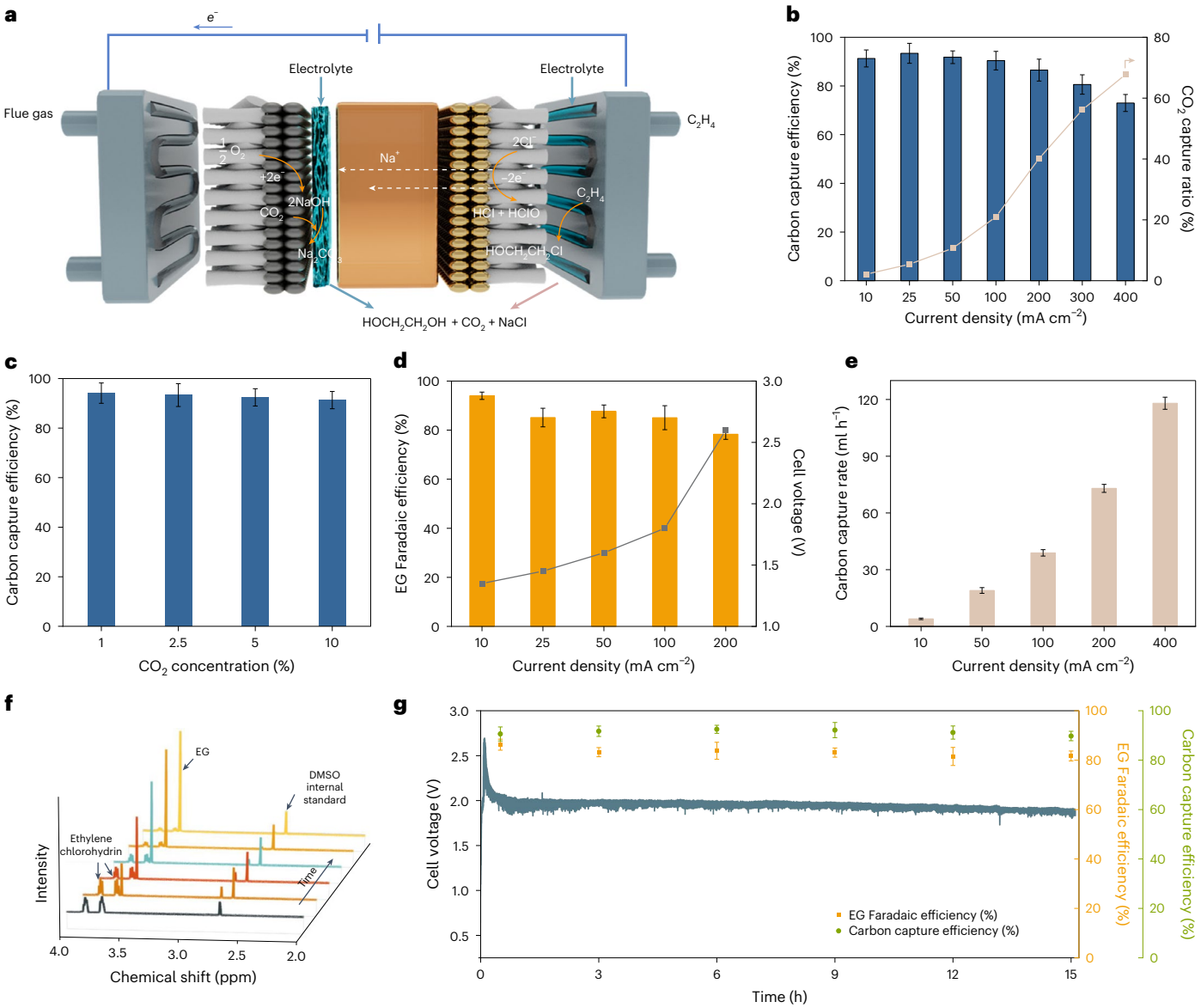

Fig. 3 | Integrating EG electrosynthesis with carbon capture. a, Integrating anodic ethylene partial oxidation with cathodic carbon capture in a cation-exchange membrane-based microfluidic electrolyser. The anode is in direct contact with membrane while there is a ~2 mm microfluidic channel between cathode and membrane to prevent salt precipitation. **b**, The performance of electrochemical carbon capture leveraging iron-single-atom catalysts at the cathode evaluated under an atmosphere of 10% CO_2 and 20% O_2, balanced with N_2. **c**, Carbon capture efficiency under conditions of 1%, 2.5%, 5% and 10% CO_2 in the inlet gas stream at 10 mA cm^{-2}. **d**, The EG Faradaic efficiency under a range of current densities and corresponding cell voltages. **e**, CO_2 regeneration rate as a function of current density. **f**, A kinetics NMR study of ethylene chlorohydrin hydrolysis to EG under neutral conditions. ^{1}H NMR spectra of ethylene chlorohydrin hydrolysis over time. **g**, The stability test of the integrated system over a span of 15 h. Data are mean and s.d. from triplicate measurements ($n = 3$).

We turned to in situ surface-enhanced Raman spectroscopy to study the binding energy of chloride ions, anticipating that this as a result of change in electronic structure and might correlate with the chloride oxidation activity. Cl adsorption on $RuSnO_x$ (271 and 335 cm^{-1}) is shifted to a lower wavenumber compared with that observed on RuO_2 (274 and 348 cm^{-1}) (Fig. 2f and Supplementary Fig. 26), indicating a weaker *Cl binding on $RuSnO_x$ relative to RuO_2.

The influence of dopants on catalytic performance was further elucidated by analysing the *p*-band centre of the the oxygen atom at the coordinatively unsaturated metal site (O_c) site. This showed a linear correlation between *p*-band centre and $\Delta G_{*O\rightarrow *OCl}$ (Supplementary Fig. 27). This suggests that Sn doping shifts the *p* bands away from the Fermi level, thereby weakening *Cl adsorption. A similar trend was observed with Bader charge analysis, where more negatively charged O_c sites in $RuSnO_x$ make it less likely to accommodate electrons from Cl^-, thus reducing the adsorption strength of *Cl on O_c (Fig. 2g). Crystal orbital Hamilton population (COHP) analysis accords with this picture, for it shows a stronger Ru–O_c bond in $RuSnO_x$, characterized by a shorter bond length and a lower integrated COHP value, this linked to weaker O_c–Cl binding (Fig. 2h).

Integrating EG synthesis from ethylene with carbon capture

We integrated chloride-mediated ethylene oxidation with carbon capture in a cation-exchange membrane-based microfluidic electrolyser (Fig. 3a). The anode is in direct contact with membrane while there is a ~2 mm microfluidic channel between cathode and membrane to prevent salt precipitation. When it was fed by using a 10% CO_2 stream, the system maintained >90% CO_2 capture efficiency below 100 mA cm^{-2} current density (Fig. 3b). We further tested this down to 1% CO_2 concentration (Fig. 3c and Supplementary Fig. 28). The results reveal that at lower

https://doi.org/10.1038/s41929-025-01392-9

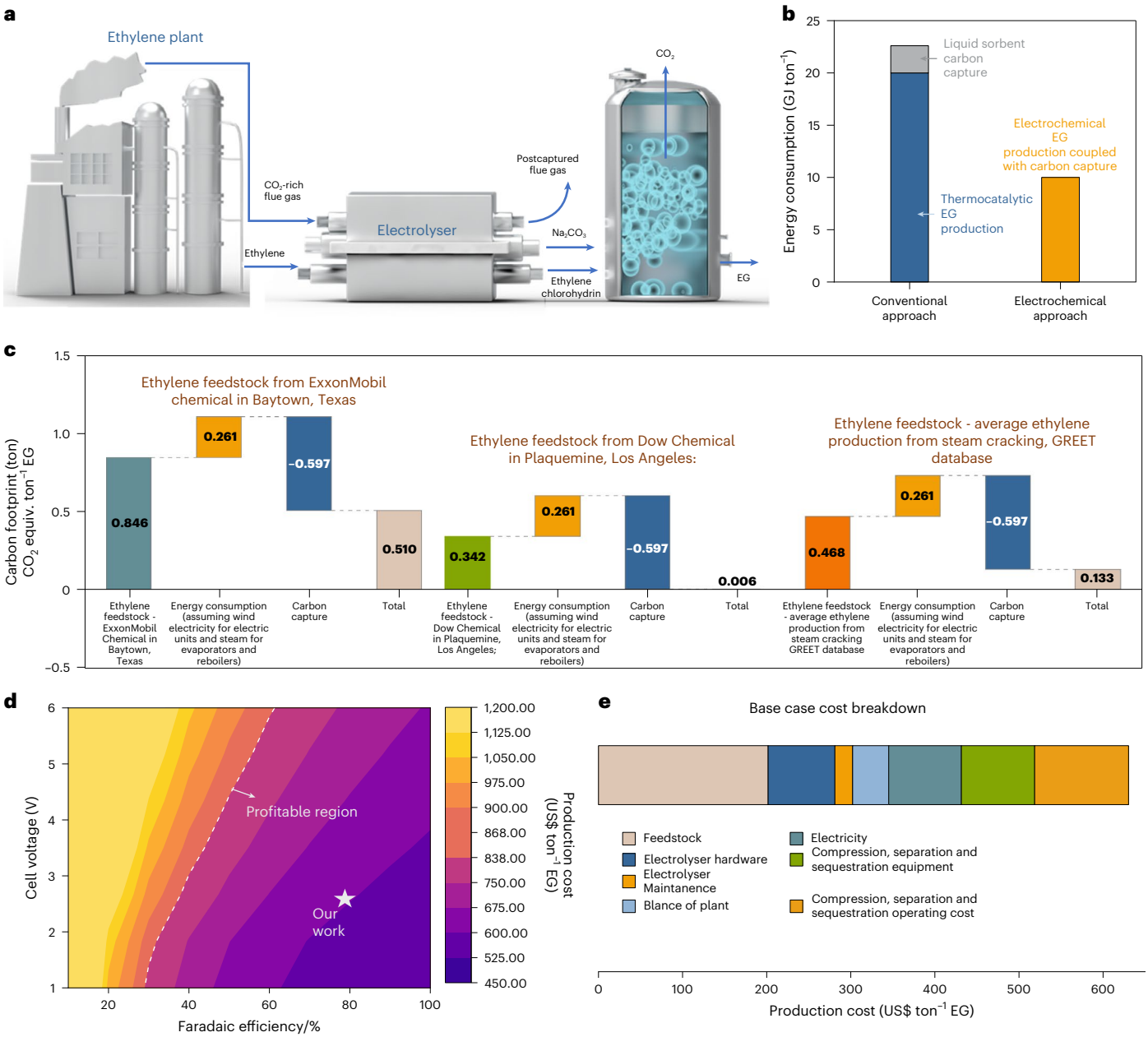

Fig. 4 | Electrified EG synthesis compared with traditional EG manufacture. **a**, The schematics of electrochemical EG production coupled with carbon capture utilizing fossil-fuel-derived ethylene. **b**, Energy consumption of EG electrosynthesis coupled with carbon capture versus today's EG manufacture, this latter presumed to be combined with liquid sorbent carbon capture. **c**, Greenhouse gas emissions of EG produced via the electrified process reported in this work, utilizing ethylene produced at different facilities and assuming wind electricity for electric units and steam from natural gas for evaporators and reboilers. **d**, Techno-economic analysis of paired EG electrosynthesis with CO_2 capture. **e**, Production cost breakdown of electrochemical EG production coupled with CO_2 capture.

current densities, carbon capture efficiency is determined by the OH^- ions generated at the cathode. At higher current densities, however, carbon capture correlates more directly with CO_2 concentration, with higher CO_2 concentrations leading to enhanced carbon capture efficiency. The system operated at a full cell voltage of 1.8 V and a current density of 100 mA cm^{-2}.

To produce EG and release the captured CO_2, we mixed—outside the electrolyser—the postcarbon capture catholyte with the anolyte. This led to hydrolysis of ethylene chlorohydrin to EG accompanied by the regeneration of CO_2 and sodium chloride (Supplementary Note 5). The regenerated CO_2 was measured using a water displacement method. EG production rates ranged from 180 μmol h^{-1} cm^{-2} at 10 mA cm^{-2}, accompanied by 94% Faradaic efficiency, to 1,600 μmol h^{-1} cm^{-2} at 100 mA cm^{-2} at 85% Faradaic efficiency (Fig. 3d) and CO_2 was regenerated at 4–118 ml $h^{-1}cm^{-2}$ (Fig. 3e and see Supplementary Table 4 for a comparison with previous literatures). In situ kinetic NMR showed that 95% conversion was achieved from {ethylene chlorohydrin and sodium carbonate} to {EG and CO_2} (Fig. 3f). Active chlorine species were not detected in the liquid products nor in the regenerated CO_2 stream. Extending the hydrolysis time to 6 h increased the overall conversion to 99%. We tested the integrated system at 100 mA cm^{-2} for 15 h (Fig. 3g), finding that the voltage remained in the range 1.85–1.89 V, that the Faradaic efficiency to EG remained above 81% and that the carbon capture efficiency was stable in the range of 89–92%. High-resolution transmission electron microscopy (TEM) characterization and energy dispersive spectroscopy mapping of $RuSnO_x$ were carried out, these

data indicating that morphology is retained following stability tests (Supplementary Figs. 29 and 30).

Ethylene production is a major source of greenhouse gas emissions, with major US facilities emitting 0.69–1.88 tonnes of CO_2 per tonne of ethylene produced[21]. There is notable opportunity to integrate the electrified system reported in this work with traditional ethylene production to synthesize EG from ethylene while capturing CO_2 from flue gas (Fig. 4a). The process flow diagram of electrochemical EG production coupled with carbon capture is presented in Supplementary Fig. 31, and the mass balance can be found in Supplementary Table 5 (Supplementary Notes 6 and 7). Using fossil-fuel-derived ethylene, the electrified system can sequester 0.60 tonnes of CO_2 per tonne of EG and requires only 10.0 GJ of energy per tonne—compared with the 22.6 GJ needed for conventional thermocatalytic processes (Fig. 4b). Using greenhouse gas emissions data from the GREET database for average US ethylene production via steam cracking, the production of one tonne of EG involves greenhouse gas emissions of 0.468 tonnes CO_2 equiv. from the ethylene feedstock alone[22]. If we assume wind electricity (2.86 kg CO_2 equiv. per gigaJoule) for electric units and steam from natural gas (78.17 kg CO_2 equiv. per gigaJoule) for reboilers and evaporators, the electrified system reduces the cradle-to-gate greenhouse gas emissions to 0.133 tonnes CO_2 equiv. per tonne of EG, compared with the global average of 1.2 tonnes CO_2 equiv. (Fig. 4c). Greenhouse gas emissions from this process vary between 0.006 and 0.510 tonnes CO_2 per tonne of EG, depending on the ethylene source. Techno-economic analysis indicates that the electrified system is capable of producing EG at an estimated cost of US$630 per tonne, which is competitive with the current market prices of US$800 to US$1,200 per tonne (Fig. 4d and Supplementary Note 8). Key cost factors include feedstock, compression, separation and sequestration, as well as electricity and electrolyser hardware (Fig. 4e). The adoption of cost-effective catalysts such as Fe–N–C and $RuSnO_x$, replacing traditional materials such as Pt/C and IrO_2 in proton exchange membrane (PEM) electrolysers, could further reduce the cost of electrolyser, potentially bringing the production cost of EG down to US$580 per tonne (Supplementary Fig. 32).

Conclusion

In this study, we demonstrate an electrochemical method for EG production from ethylene coupled with carbon capture in a single electrolyser. The in situ photoluminescence analysis revealed that the pH gradient across the electrolyser membrane created a near-neutral microenvironment at the membrane–catalyst interface that adversely impacts ethylene oxidation efficiency. Seeking to address this, we integrated carbon capture at the cathode to mitigate OH^- diffusion and developed a tin-doped ruthenium oxide catalyst to enhance ethylene oxidation selectivity. In situ XAS, surface-enhanced Raman spectroscopy coupled with DFT calculations suggest that tin doping increases the stability and activity of $RuSnO_x$ by tuning the oxidation state of ruthenium and promoting *Cl adsorption over *OH, thereby shifting selectivity towards chloride-mediated ethylene oxidation. The optimized system achieves 94% EG Faradaic efficiency and 91% carbon capture efficiency in a 10% CO_2 stream. The integrated system requires 10.0 GJ of energy per tonne EG produced and sequesters 0.6 tonnes of CO_2, compared with the traditional 22.6 GJ. A cradle-to-gate analysis indicates that this approach can lower the greenhouse gas emissions of EG production from fossil-fuel-derived ethylene to 0.133 tonnes CO_2 equiv. per tonne EG.

Methods

Synthesis of Fe–N–C catalyst

In a typical synthesis of N-doped carbon, a 400 ml methanol solution containing 9.04 g of $Zn(NO_3)_2{\cdot}6H_2O$ was poured into another 400 ml methanol solution containing 10.507 g of 2-methylimidazole, while stirring quickly. The mixture was stirred for 2 min and then kept in a stable condition for 1 day without further stirring. Afterwards, the white precipitates were collected by centrifugation, washed with methanol three times and dried in a vacuum oven at 70 °C. To obtain N-doped carbon, the synthesized zeolitic imidazolate framework (ZIF-8) powders were ground and then subjected to heat treatment at 900 °C for 1 h under Ar purging conditions in a tube furnace. Subsequently, we dispersed 200 mg of N-doped carbon in 40 ml of H_2O and sonicated it for 20 min. Then, 1 ml of $Fe(NO_3)_3$ solution (prepared by dissolving 269.3 mg of iron nitrate in 10 ml of H_2O) was added to the dispersion and subjected to an additional 20 min of sonication, followed by continuous stirring for 24 h. After filtration, the resulting precipitate was rinsed with deionized water and dried in a vacuum oven overnight. In the final step, the dried sample was pyrolysed in the tube furnace at 1,000 °C for 2 h under an Ar atmosphere.

Materials characterization

Morphological characterization of the synthesized sample was performed by using TEM (JEOL JEM-2100F) at an acceleration voltage of 200 kV. High-angle annular dark field-scanning TEM and energy dispersive spectroscopy analysis were obtained in the JEOL JEM-2100F (JEOL) microscope. X-ray photoelectron spectroscopy data were measured by NEXSA G2 (Thermo Fisher Scientific). X-ray absorption near-edge spectroscopy (XANES) and extended X-ray absorption fine structure were performed at the Pohang Accelerator Laboratory (PAL) 8C beamline.

Electrochemical characterization

The electrocatalytic performance for the ORR was evaluated using a rotating disc electrode (Pine Instrument) system within a three-electrode setup. The counter electrode and reference electrode employed were a glassy carbon rod and an Ag/AgCl electrode, respectively. The working electrode was a 5 mm (0.19625 cm^2) glassy carbon disk electrode. All potentials are reported relative to the RHE, determined by measuring the equilibrium potential of hydrogen oxidation/evolution under an H_2-saturated electrolyte using a Pt electrode. ORR activity was measured using linear scan voltammetry at a rotation speed of 1,600 rpm and a scan rate of 10 mV s^{-1}, in an O_2-saturated 0.1 M KOH electrolyte. The capacitance arising from non-Faradaic effects was compensated for by measurements conducted under Ar-saturated conditions, and iR-correction was applied.

Electrode preparation

To fabricate $RuSnO_x$-coated Ti electrode, titanium felt is treated in 0.5 M oxalic acid (98%, Sigma-Aldrich) at 80 °C for 30 min, washed by deionized water and dried in the vacuum oven. A painting solution of 0.02 mM ruthenium chloride hydrate (99.9%, Sigma-Aldrich) and 0.02 mM tin chloride hydrate (98%, Sigma-Aldrich) in isopropanol was prepared with a Ru:Sn molar ratio of 1:1. This solution was applied to the pretreated titanium substrate using an airbrush with a loading of 2 mg cm^{-2}. The loading is determined by measuring the mass difference. Subsequently, the coated samples were dried at 100 °C for 10 min in an oven and then sintered at 450 °C for 1 h in a furnace. For cathode, the catalyst ink was prepared by mixing the catalyst with Nafion ionomer (5 wt%, Ion Power) and isopropanol (Sigma-Aldrich). The catalyst loading of the Fe–N–C catalyst was 2 mg cm^{-2}. The catalysts were sprayed onto Ag-sputtered porous polytetrafluoroethylene (PTFE) membrane using a spray gun as a gas diffusion electrode. Ag/PTFE gas diffusion layer was prepared by sputtering a 300-nm-thick Ag layer onto a PTFE membrane (average pore size of 450 nm) using a Ag target (99.99%) at a rate of 1 Å s^{-1}.

RRDE experiment

The RRDE setup is used to differentiate the current densities for the oxygen evolution reaction and the chloride oxidation reaction. To quantify chloride oxidation rates during the electrolysis process, we utilize an RRDE setup featuring a platinum ring electrode and a glassy

carbon disk electrode. The potential of the Pt ring electrode is fixed at 0.95 V, which enables the accurate quantification of active chlorine species at the ring through their reduction back to Cl^-. The collection efficiency for these active chlorine species is denoted as N_l, which is determined by the electrode area. Based on these parameters, the partial current density for chloride oxidation can subsequently be calculated by $i_{CER} = \frac{i_{ring}}{N_l}$. In a typical RRDE test, 5 mg of catalyst was added to 1 ml of isopropyl alcohol and 20 µl of Nafion ionomer (5%; fuel cell store) and sonicated for 1 h to obtain a well-dispersed catalyst ink. For electrode preparation, 16 µl of catalyst ink was drop-cast onto the glassy carbon disk electrode, resulting in a catalyst loading of 0.4 mg cm^{-2} and then dried at room temperature before usage. A graphite electrode and an Ag/AgCl electrode were used as the counter and reference electrode, respectively. The rotation rate is set to 2,500 rpm.

Ethylene partial oxidation coupled with carbon capture

The ethylene partial oxidation was first tested using a MEA-based electrolyser with an active area of 1 cm^2. The cell incorporated a ruthenium-based mixed oxide as the anodic catalyst. A reinforced cation-exchange membrane (DF2807, Dongyue Polymer Material) was used to separate the cathodic and anodic chambers. The lab-synthesized iron single-atom catalysts or 40% Pt on Vulcan XC72 (fuel cell store) were used as catalysts for oxygen reduction reaction and carbon capture. A total of 1 M NaCl is fed as an electrolyte on both sides. After switching to the ethylene oxidation paired with carbon capture, the anode remains in direct contact with the membrane, while a 2 mm microfluidic channel (Supplementary Fig. 33) was introduced between cathode and membrane to remove the carbonate and prevent salt precipitation. Various concentrations of CO_2 are fed to the cathodic gas chamber with 20% oxygen and nitrogen is used as the balanced gas. Ethylene is fed to the anodic gas chamber for ethylene partial oxidation. A constant volume (25 ml) of catholyte and anolyte was circulated through the electrolyser at a stable flow rate of 10 ml min^{-1} controlled by two peristaltic pumps. The CO_2 capture efficiency is defined as the ratio of the number of OH^- that converts CO_2 to carbonate to the number of cathodically generated hydroxide ions. The amount of captured CO_2 was determined by subtracting the CO_2 measured in the outlet of the cathodic chamber (via GC injection) from the CO_2 fed into the electrolyser. The number of cathodically generated hydroxide ions was calculated by the current density. After the experiment, the anolyte samples were collected to measure the ethylene chlorohydrin formation. Then the anolyte was mixed with catholyte, to measure the EG formation and CO_2 regeneration. The regenerated CO_2 was measured using a water displacement method. The liquid products were analysed by NMR spectrometry using DMSO as an internal standard via a presaturated water suppression method. A typical procedure to prepare an NMR sample is to add 0.1 ml 0.008 M DMSO in D_2O solution and 0.4 ml D_2O to 0.1 ml liquid sample.

In situ photoluminescence study

To evaluate the local pH at the interface of the catalyst and the membrane in the MEA, we affixed a pH-sensitive dye, LysoSensor Green DND 189 (LSG), to the membrane and executed an in situ photoluminescence study[23]. We employed an ultraviolet torch at 385 nm to collect fluorescence emissions via a spectrometer (Ocean Optics, QE Pro). The dyes were calibrated using solutions of varying pH levels (1–7) to determine their fluorescence, with 100 µM of the dyes dissolved in the solutions, and photoluminescence spectra of the standards were collected in a cuvette using a spectrometer (Ocean Optics, QE Pro), fibre-coupled ultraviolet light-emitting diode (Ocean Optics) and a cuvette holder (Ocean Optics). LSG demonstrated fluorescence emission between 500 and 575 nm at a pH range of 1–7. Consequently, alterations in pH at the membrane interface can be examined by monitoring the peak shifts of the pH-sensitive dyes.

In situ kinetics NMR measurement

The in situ kinetics NMR study is carried out using a 400 MHz Bruker Avance III HD Nanobay system. The ethylene chlorohydrin obtained from the electrochemical chloride-mediated ethylene partial oxidation was collected, which was then subjected to alkaline and neutral conditions by introducing stoichiometric amounts of sodium hydroxide and sodium bicarbonate. We used postelectrolysis ethylene chlorohydrin solution with a pH of 1.5 as our control experiment. Dimethyl sulfoxide in deuterium water is used as an internal standard. The one-dimensional ^1H spectrum was acquired every 2 min to monitor the hydrolysis of ethylene chlorohydrin employing water suppression via a pre-saturation method.

DFT calculations

In this work, all DFT calculations were performed with periodic slab models using the Vienna ab initio simulation package (VASP)[24–27]. The Perdew–Burke–Ernzerhof[28] exchange-correlation functional was used. The projector-augmented wave method was utilized to describe the electron-ion interactions, and the cut-off energy for the plane-wave basis set was 520 eV. All the configurations were optimized using a force-based conjugate gradient algorithm. We employed the D3 correction method proposed by Grimme et al.[29] to correct the long-range dispersion interactions between the adsorbates and catalysts. Dipole correction[30] was also considered to correct the electrostatic interaction resulting from the periodic images. The COHP analysis was performed using the Lobster 5.1.0 package[31]. The atomic coordinates of the optimized structures are provided in the Supplementary Data.

Techno-economic analysis and life cycle assessment

The process is simulated using Aspen Plus V14.0 and the process flow diagram is presented in Supplementary Fig. 31, and the mass balance can be found in Supplementary Table 5. The capital cost and operating cost for compression, separation and CO_2 sequestration are calculated using Aspen Plus economic analyser. The system boundary of life cycle assessment includes feedstocks, investigated processes and utility. Two scenarios were considered for the assessment: assuming wind electricity for all unit operations and assuming wind electricity for electrically powered units and steam for evaporator and reboiler. The LCA data are from GREET 2023 (Argonne National Laboratory). The results are summarized in Supplementary Tables 6 and 7. The techno-economic analysis was performed based on previously reported methods[32,33]. The model's parameters are detailed in the Supplementary Table 8. The techno-economic analysis analysis incorporates a 20-year operational period, accounting for both capital and operational expenses. In the model, we considered capital cost, installation cost, balance of plant, input chemical cost, electricity cost, operational cost, maintenance cost and separation cost. All prices are in US dollars unless stated otherwise. Additional details can be found in Supplementary Notes 6–8 and Supplementary Tables 4–9.

Data availability

All other data supporting the findings of the study are available from the corresponding authors upon reasonable request. Source data are provided with this paper.

References

1. Yue, H., Zhao, Y., Ma, X. & Gong, J. Ethylene glycol: properties, synthesis, and applications. *Chem. Soc. Rev.* **41**, 4218–4244 (2012).
2. Zheng, J. et al. Ambient-pressure synthesis of ethylene glycol catalyzed by C_{60} buffered Cu/SiO_2. *Science* **376**, 288–292 (2022).
3. Falcke, H. et al. Best available techniques (BAT) reference document for the production of large volume organic chemicals. *JRC Publications Repository* https://doi.org/10.2760/77304 (Publications Office of the European Union, 2017).

4. Rebsdat, S. & Mayer, D. in *Ullmann's Encyclopedia of Industrial Chemistry* (ed. Ley, C.) 531–546 (Wiley-VCH, 2000).
5. Xia, R. et al. Electrosynthesis of ethylene glycol from C_1 feedstocks in a flow electrolyzer. *Nat. Commun.* **14**, 4570 (2023).
6. Lum, Y. et al. Tuning OH binding energy enables selective electrochemical oxidation of ethylene to ethylene glycol. *Nat. Catal.* **3**, 14–22 (2020).
7. Mynko, O. et al. Reducing CO_2 emissions of existing ethylene plants: evaluation of different revamp strategies to reduce global CO_2 emission by 100 million tonnes. *J. Clean. Prod.* **362**, 132127 (2022).
8. Ghanta, M., Fahey, D. & Subramaniam, B. Environmental impacts of ethylene production from diverse feedstocks and energy sources. *Appl. Petrochemical Res.* **4**, 167–179 (2014).
9. Qian, H. et al. The comparative life-cycle environmental effects of chemical feedstock change driven by energy system transition: a case study from China's ethylene glycol industry. *J. Clean. Prod.* **355**, 131764 (2022).
10. Xu, S. et al. Comparative life cycle assessment of energy consumption, pollutant emission, and cost analysis of coal/oil/biomass to ethylene glycol. *ACS Sustain. Chem. Eng.* **9**, 15849–15860 (2021).
11. De Luna, P. et al. What would it take for renewably powered electrosynthesis to displace petrochemical processes? *Science* **364**, eaav3506 (2019).
12. Rocha, R. S., Lanza, M. R. V. & Bertazzoli, R. Electrosynthesis of ethylene glycol from oxidation of ethylene using a TiO_2–RuO_2/PTFE gas diffusion electrode. *Electrocatalysis* **2**, 273–278 (2011).
13. Li, X., Zhao, X., Liu, Y., Hatton, T. A. & Liu, Y. Redox-tunable Lewis bases for electrochemical carbon dioxide capture. *Nat. Energy* **7**, 1065–1075 (2022).
14. Bui, J. C. et al. Analysis of bipolar membranes for electrochemical CO_2 capture from air and oceanwater. *Energy Environ. Sci.* **16**, 5076–5095 (2023).
15. Seo, H. & Hatton, T. A. Electrochemical direct air capture of CO_2 using neutral red as reversible redox-active material. *Nat. Commun.* **14**, 313 (2023).
16. Voskian, S. & Hatton, T. A. Faradaic electro-swing reactive adsorption for CO_2 capture. *Energy Environ. Sci.* **12**, 3530–3547 (2019).
17. Jin, S., Wu, M., Jing, Y., Gordon, R. G. & Aziz, M. J. Low energy carbon capture via electrochemically induced pH swing with electrochemical rebalancing. *Nat. Commun.* **13**, 2140 (2022).
18. Zhu, P. et al. Continuous carbon capture in an electrochemical solid-electrolyte reactor. *Nature* **618**, 959–966 (2023).
19. Sandin, S., Karlsson, R. K. B. & Cornell, A. Catalyzed and uncatalyzed decomposition of hypochlorite in dilute solutions. *Ind. Eng. Chem. Res.* **54**, 3767–3774 (2015).
20. Yi, C., Zou, J., Yang, H. & Leng, X. A facile hydrothermal synthesis of graphene/RuO_2/Co_3O_4 nanocomposites with high pseudocapacity. *N. J. Chem.* **42**, 7066–7072 (2018).
21. Greenhouse gas emissions rate of major ethylene producing facilities in the United States. https://www.statista.com/statistics/1011977/ghg-emissions-rate-major-ethylene-producing-facilities-by-company/ (CIEL, 2019).
22. Greenhouse gases, regulated emissions, and energy use in technologies model. https://greet.anl.gov/ (Argonne National Laboratory, 2023).
23. Lee, G. et al. CO_2 electroreduction to multicarbon products from carbonate capture liquid. *Joule* **7**, 1277–1288 (2023).
24. Kresse, G. & Furthmüller, J. Efficient iterative schemes for ab initio total-energy calculations using a plane-wave basis set. *Phys. Rev. B* **54**, 11169–11186 (1996).
25. Kresse, G. & Furthmüller, J. Efficiency of ab-initio total energy calculations for metals and semiconductors using a plane-wave basis set. *Comput. Mater. Sci.* **6**, 15–50 (1996).
26. Kresse, G. & Hafner, J. Ab initio molecular-dynamics simulation of the liquid-metal–amorphous-semiconductor transition in germanium. *Phys. Rev. B* **49**, 14251–14269 (1994).
27. Kresse, G. & Hafner, J. Ab initio molecular dynamics for liquid metals. *Phys. Rev. B* **47**, 558–561 (1993).
28. Perdew, J. P., Burke, K. & Ernzerhof, M. Generalized gradient approximation made simple. *Phys. Rev. Lett.* **77**, 3865 (1996).
29. Grimme, S., Antony, J., Ehrlich, S. & Krieg, H. A consistent and accurate ab initio parametrization of density functional dispersion correction (DFT-D) for the 94 elements H-Pu. *J. Chem. Phys.* **132**, 154104 (2010).
30. Dominguez-Ramos, A., Singh, B., Zhang, X., Hertwich, E. G. & Irabien, A. Global warming footprint of the electrochemical reduction of carbon dioxide to formate. *J. Clean. Prod.* **104**, 148–155 (2015).
31. Nelson, R. et al. LOBSTER: local orbital projections, atomic charges, and chemical-bonding analysis from projector-augmented-wave-based density-functional theory. *J. Comput. Chem.* **41**, 1931–1940 (2020).
32. Jouny, M., Luc, W. & Jiao, F. General techno-economic analysis of CO_2 electrolysis systems. *Ind. Eng. Chem. Res.* **57**, 2165–2177 (2018).
33. Jin, J. et al. Constrained C_2 adsorbate orientation enables CO-to-acetate electroreduction. *Nature* **617**, 724–729 (2023).

Acknowledgements

This research was supported by Braskem. This research utilized the EPIC, Keck-II and SPID facilities at Northwestern University's NUANCE Center. The Center is supported by the ShyNE Resource, funded by the NSF ECCS-2025633, the IIN and the Materials Research Science and Engineering Center (MRSEC) programme of Northwestern University, under NSF grant no. DMR-2308691. We thank the Canadian Light Source (the HXMA beamline, 06ID) for providing beamtime (proposal no. 38G13481) and extend our gratitude to N. Chen and W. Chen from the HXMA beamline for their guidance. The DFT calculations of this work were supported through computational resources and staff contributions provided for the Quest high-performance computing facility at Northwestern University which is jointly supported by the Office of the Provost, the Office of Research and Northwestern University Information Technology.

Author contributions

R.X. conceived the idea and designed the experiments. Y.C and Y.C. performed the DFT calculation. R.X., H.S. and H.Z. carried out the catalyst synthesis and characterization. H.L. helped with gas product quantification. P.O. helped with the DFT calculation. R.D., S.P., P.P. and Z.G. helped with XAS experiment. R.X., E.M., M.R., M.N. and R.D. engaged in process development and TEA and LCA analysis. Y.L. helped with the in situ photoluminescence study. R.X. prepared the first draft. K.X. and E.H.S. revised the manuscript. D.Z., W.N., C.T., Y.C., C.Y. and O.F. engaged in discussion and manuscript revision. E.H.S. supervised the whole project.

Competing interests

There is a US provisional patent application (no. 63/607,143) titled 'Methods and systems for electrolysing hydrocarbons coupled with CO_2 capture' filed by the authors R.X., K.X. and E.H.S. and their institutions. Another US provisional patent application titled 'System for producing mono-EG and carbon dioxide and method for producing same' is filed by the authors R.X., K.X., E.H.S., E.M., M.R., M.N. and R.D. The other authors declare no competing interests.

Additional information

Supplementary information The online version contains supplementary material available at https://doi.org/10.1038/s41929-025-01392-9.

Correspondence and requests for materials should be addressed to Ke Xie or Edward H. Sargent.

Peer review information *Nature Catalysis* thanks Jonggeol Na, Haotian Wang and Yan Zhao for their contribution to the peer review of this work.